Canadian banknotes to explore the phenomenon of diffraction

Isabelle Bonnet, Julien Gabelli

▶ **To cite this version:**

Isabelle Bonnet, Julien Gabelli. Canadian banknotes to explore the phenomenon of diffraction. European Journal of Physics, 2024, 45 (3), pp.035302. 10.1088/1361-6404/ad2fd8 . hal-04518351

HAL Id: hal-04518351
https://hal.science/hal-04518351v1

Submitted on 26 Mar 2024

HAL is a multi-disciplinary open access archive for the deposit and dissemination of scientific research documents, whether they are published or not. The documents may come from teaching and research institutions in France or abroad, or from public or private research centers.

L'archive ouverte pluridisciplinaire **HAL**, est destinée au dépôt et à la diffusion de documents scientifiques de niveau recherche, publiés ou non, émanant des établissements d'enseignement et de recherche français ou étrangers, des laboratoires publics ou privés.

Distributed under a Creative Commons Attribution 4.0 International License

Canadian banknotes to explore the phenomenon of diffraction

Isabelle Bonnet[1] **& Julien Gabelli**[2]

[1]Institut Curie, Université PSL, Sorbonne Université, CNRS UMR168, Physics of Cells and Cancer, 75005 Paris, France

[2]Laboratoire de Physique des Solides, Université Paris Saclay, CNRS UMR 8502, Batiment 510, 91 405 Orsay, France

E-mail: julien.gabelli@u-psud.fr

Abstract. Grating and its well-known diffraction pattern are the basis of spectrometers to characterize light sources. Reciprocally, periodic peaks in the diffraction pattern of X-rays scattered by solids bring valuable information about the internal geometry of the crystal lattice, providing details about the arrangement of atoms in the solid. In both cases, periodic gratings are considered. What about non-periodic gratings? Is it possible to reconstruct any grating structure knowing its diffraction pattern? We answer this question by studying diffraction through the hologram hidden in a Canadian banknote. We measure the diffraction of near-infrared light to numerically reconstruct the grating structure using the Gerchberg-Saxton algorithm. We then compare this reconstructed grating structure with the picture of the grating structure observed with a phase-contrast microscope. Such an approach allows us to study diffraction from a perspective different from that usually taught at university.

Keywords: Diffraction, Fast Fourier Transform, Gerchberg-Saxton algorithm, Diffractive phase hologram.

DOI: https://doi.org/10.1088/1361-6404/ad2fd8

Submitted to: *Eur. J. Phys.*

1. Introduction

Although the first paper money was used in China as early as the 7^{th} century, banknotes did not appear in Europe until the 16^{th} century [1, 2]. If the bills were originally hand-written on banknote paper, they now use modern printing techniques to make the task of counterfeiter more difficult [3]. The modern standard techniques include images that combine technical complexity with visual simplicity, watermarks, security threads, or secure windows [4]. The first polymer banknotes appeared in the 1980s: as well as being extremely robust and durable, they have enabled the development of highly complex diffractive holograms that cannot be seen by the naked eye. These holograms are a new type of security that is extremely complicated to reproduce due to their intricate and

complex nature [5]. Australia has been the first country to propose a polymer banknote with a diffraction grating to deter counterfeiting [6, 7].

The theory of diffraction by periodic structures is of fundamental importance as it is the building block of spectrometers and the basis of X-ray crystallography [8]. The X-ray diffraction enabled us to understand the internal geometry of crystals [9, 10] and played a key role in the discovery of the double-helix structure of DNA [11]. The diffraction gratings studied in textbooks are usually transmission gratings with periodic surface grooves to create a simple diffraction pattern that perfectly illustrates the diffraction formula and its different diffractive orders [12]. Understanding the different orders of diffraction allows us to determine the structure of a grating from its diffraction pattern. The reciprocal is rarely addressed in the classroom: what grating should be used to obtain a given diffraction pattern? The study of the diffractive hologram of a Canadian banknote enables us to address this question.

The article is organized as follows. (i) First, we observe the Fraunhofer diffraction pattern of a $5 banknote hologram with a laser. (ii) Using Gerchberg-Saxton's (GS) algorithm [13], we numerically compute a phase grating using an image of the Fraunhofer diffraction pattern. (iii) Then, we image the hologram with a phase-contrast microscope and perform its fast Fourier transform (FFT) [14] to compute the corresponding diffraction pattern. (iv) We finally compare the numerically reconstructed phase grating to the one we imaged.

Note that the quantitative experiments described below have been performed using materials from a university laboratory. However, a laser pointer is enough to reveal the diffraction pattern of banknotes, as presented on several websites [15, 16].

2. Fraunhofer pattern of the banknote diffractive hologram

The set of Canadian polymer banknotes contains diffractive holograms hidden in the maple leaf located at the corner of the note (Figure 1(a)). In this first section, we observe the Fraunhofer diffraction pattern of the phase grating hidden in the maple leaf of a $5 banknote by illuminating it with a laser.

2.1. Experimental setup

The experimental setup is shown in Figure 1(b). We use a 2.5 cm diameter circular piece from a $5 bill. The light source is a Thorlabs laser diode L785P090 ($\lambda = 785$ nm) coupled to a single-mode optical fiber (780 - 970 nm). A fiber collimation package with numerical aperture NA = 0.15 and a focal $f = 18.4$ mm collimates light from the fiber. We assume the light output from the optical fiber is a Gaussian free-space collimated beam with amplitude $A_0(x, y) = \sqrt{I_0} \exp\left[-\frac{x^2+y^2}{w^2}\right]$ where (x, y) are the coordinates in the plane

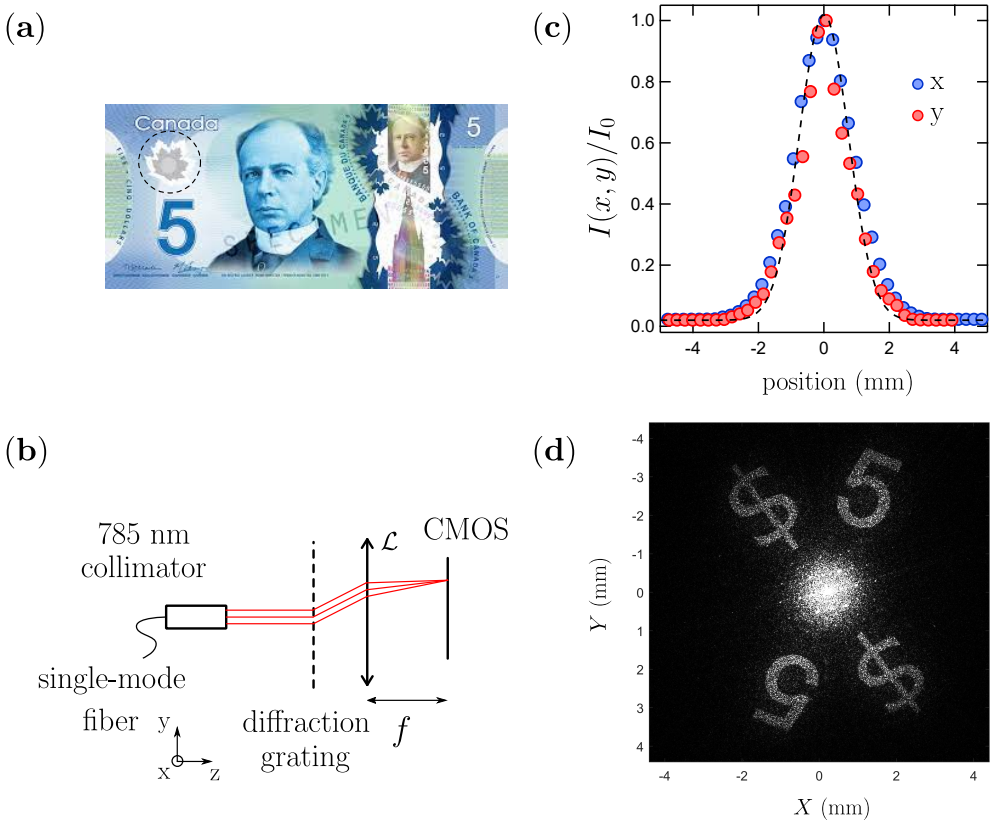

Figure 1. **(a)** Canadian five-dollar note, ©Bank of Canada [17]. We use a circular piece around the frosted maple leaf shape and adjust it in a one-inch optic mount (black dashed circle). **(b)** Schematic of the experimental setup. The collimator is used to bring the laser beam to a parallel configuration and the CMOS camera is located at the focal plane of the lens $\mathcal{L}$. **(c)** Intensity $I(x, y)$ of the Gaussian beam in the x (blue markers) and y (red markers) direction normalized to the maximum intensity I_0. The waist is given by the width at half-maximum. **(d)** Fraunhofer diffraction pattern observed at the focal plane of $\mathcal{L}$.

perpendicular to the beam axis, I_0 is the laser intensity, and w is the beam waist. We characterize it with a CMOS ASI183mm Zwo camera located between the collimation package and the hologram: we estimate the beam waist diameter $w \simeq 1.6\,\text{mm}$ (Figure 1(c)). The Gaussian approximation is valid, thereby confirming the suitability of the subsequent numerical approach. The same camera is placed in the back focal plane of a lens $\mathcal{L}$ of focal length $f = 75\,\text{mm}$ to observe the Fraunhofer diffraction pattern, shown in a 3673×3673 sampled image (Figure 1(d)). This pattern reveals the value of the bill: two \$5 positioned crosswise.

2.2. Fraunhofer diffraction theory

Diffraction occurs when light passes through an aperture of a size comparable to its wavelength. Huygens postulated that each surface element of a diffracting aperture was a "secondary source" of a spherical wavelet of amplitude proportional to that of the inci-

dent wave. This principle can be derived from Kirchoff's integral formula on a rigorous basis assuming that the characteristic dimensions of the diffracting aperture are large compared with the wavelength [18]. The optical field at the observation point can be written as the sum of spherical waves radiated by each point of the diffractive aperture. Each of these waves has an amplitude proportional to the amplitude of the incident wave, multiplied by a purely geometric factor describing the inclination of the light rays with respect to the normal of the aperture. Starting from the Huygens approach, Augustin-Jean Fresnel proposed a mathematical model to calculate the diffraction pattern created by waves passing through an aperture, when the distances between the diffracting object, the light source, and the observation plane are comparable to the wavelength of light. Fresnel diffraction is thus an approximation for near-field diffraction and treats the wavefront as a curved surface. The Fresnel integral is the Fourier transform of the field multiplied by a term, called the Fresnel propagator which depends on the distance of propagation. Fraunhofer diffraction (named after Joseph von Fraunhofer) corresponds to the opposite limit (far-field diffraction) and assumes that the wave has propagated over a sufficiently large distance. The Fraunhofer diffraction integral omits the Fresnel propagator.

In our experiment, the incident light is perpendicular to the diffractive hologram, and the diffraction pattern is observed at a sufficiently large distance from the object, as it is at the focal plane of the imaging lens $\mathcal{L}$, as shown in Figure 1(b). It is thus the case of Fraunhofer diffraction in the paraxial approximation (small-angle approximation). Under these assumptions, the complex amplitude $A(x, y)$ of the diffracted wave becomes an integral of the transparency function multiplied by the illumination beam:

$$A(x,y) = A_0(x,y) \int_{(\Sigma)} T(x_0,y_0) \exp\left[-i\frac{2\pi}{\lambda f}\left(x_0 x + y_0 y\right)\right] dx_0 dy_0, \qquad (1)$$

where λ is the wavelength of the laser, T is the complex transparency function of the diffractive grating and Σ is the hologram surface located in the (x_0, y_0) plane. Eq. 1 is the two-dimensional Fourier transform of T. Fourier analysis being at the core of the Fraunhofer diffraction, readers wishing to know more about the fundamental properties of Fourier transforms in optics can refer to [19, 20]. The diffraction pattern is given by the intensity measured by the camera $I(x, y) = |A(x, y)|^2$. Figure 1(d) shows this diffraction pattern symbolizing the value of the five-dollar banknote, in two copies and placed crosswise.

3. Reconstruction of the phase grating corresponding to the Fraunhofer diffraction pattern

We now try to numerically find the phase grating that could give the observed diffraction pattern using the GS algorithm [13].

3.1. The Gerchberg–Saxton algorithm

The GS algorithm is an iterative algorithm that converges to a phase grating whose diffraction pattern is approximately the intensity of a sampled image I_f. It uses a fast algorithm to calculate the Fourier transform implemented with $\mathcal{O}\left(n \log_2 n\right)$ operations and memories for an array of n points: the FFT algorithm [14, 21]. In our case, working with 2d images, we use 2d FFT with the MATLAB function `"fft2.m"` from Signal Processing Toolbox.

We first create a binary image I_f representing the five-dollar positioned crosswise using vector graphics software (*Inkscape*), in Arial font, to mimic the diffraction pattern. We neglect the bright central point visible in Figure 1(d) which corresponds to zeros order diffraction and does not contain the information we are looking for. This created binary image I_f is shown at the bottom corner in Figure 2.

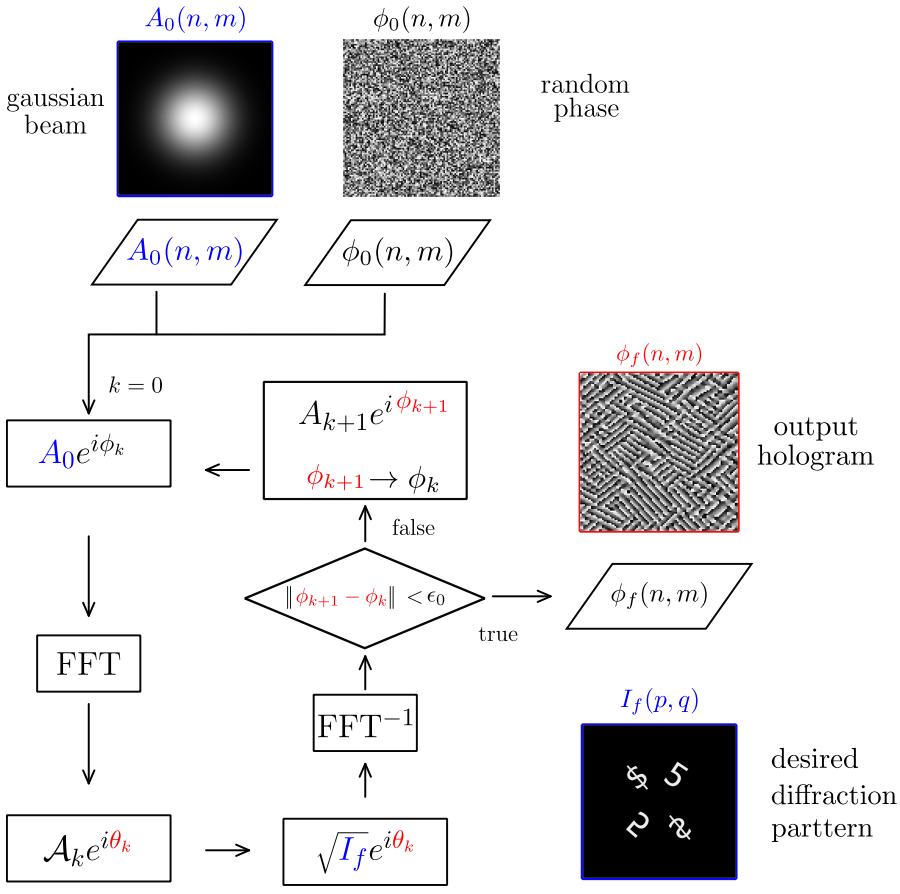

Figure 2. Flowchart associated with the Gerchberg–Saxton algorithm. A and ϕ designate amplitude and phase in real space, while $\mathcal{A}$ and θ refer to them in Fourier space.

In the following, for the sake of simplicity, we assume that complex transparency is a

phase: $T(x_0, y_0) \propto e^{i\phi(x_0,y_0)}$. The input parameters of the GS algorithm are (see eq. (2)):

- the intensity of the illuminating Gaussian beam as an image $A_0(n, m)$ of size $N \times N$ with $N = 2^{11}$ pixels giving an image width $\Delta l = 1\,\text{mm}$,
- a created binary image $I_\text{f}(p, q)$, of size $N \times N$, representing the desired diffraction pattern,
- an initial random phase for the phase grating $\phi_0(n, m)$ of size $N \times N$.

The initial phase ϕ_0 was randomly generated in $[0, 2\pi]$. The flowchart of the algorithm is shown in Figure 2. The initial field in the lens focal plane is calculated by computing the FFT of the complex field in the grating plane $A_0 e^{i\phi_0}$ where $I_0 = |A_0|^2$ is the intensity of the Gaussian laser beam (first iteration). We then compute the Fourier transform $\mathcal{A}_{p,q}$ of the complex field amplitude $A_{n,m}$ and its inverse Fourier transform by using the 2d FFT algorithm:

$$\left| \begin{array}{l} \mathcal{A}_{p,q} = \text{FFT}\,[A] = \sum_{n=1}^{N} \sum_{m=1}^{N} A_{n,m} e^{-2i\pi\left(\frac{np}{N}+\frac{mq}{N}\right)} \delta x^2, \\ A_{n,m} = \text{FFT}^{-1}\,[\mathcal{A}] = \sum_{p=1}^{N} \sum_{q=1}^{N} \mathcal{A}_{p,q} e^{2i\pi\left(\frac{np}{N}+\frac{mq}{N}\right)} \delta X_k^2, \end{array} \right. \tag{2}$$

where $X_{k0} = N \times \delta X_k$ is the spatial dimension of the image in the back-focal plane (width of the binary image I_f) and $x_0 = \frac{f\lambda}{\delta X_k}$ is the spatial dimension of the diffractive hologram. The magnitude of the calculated amplitude $|A_k|$ is substituted by the target amplitude $\sqrt{I_\text{f}}$ where I_f corresponds to the wanted picture I_f. A_k is a $2^{11} \times 2^{11}$ image of length $\Delta L = \frac{\lambda}{\pi} \frac{Nf}{\Delta l}$ mm. The new complex amplitude $\sqrt{I_\text{f}} e^{i\theta_k}$ is propagated back to the pupil plane by the inverse FFT^{-1} which gives a new magnitude A_{k+1} and a new phase ϕ_{k+1}. The algorithm is then repeated considering the diffraction by the grating $A_0 e^{i\phi_{k+1}}$. The process is repeated until the error $\epsilon = \frac{2\||\mathcal{A}_{p,q}|^2 - I_\text{f}(p,q)\|}{\||\mathcal{A}_{p,q}|^2 + I_\text{f}(p,q)\|} < \epsilon_0$ with ϵ_0 defined by the user and $\|\cdot\|$ is the Euclidean norm of the matrix. The output is a phase-diffraction pattern $\phi_\text{f}(n, m)$ of size $N \times N$.

3.2. Case of the Canadian banknote

Using the diffraction pattern representing the five-dollar positioned crosswise we have created, the phase grating obtained with the GS algorithm is shown in Figure 3(a). As expected, the FFT of this calculated grating illuminated with the Gaussian beam gives the diffraction pattern displayed in Figure 3(b), which looks like the experimental one (Figure 1(d)), except for the central spot, which was not considered in the binary image.

Convergence of the GS algorithm takes 25 minutes on a personal computer with an Intel i7-8650U processor and 16 GB RAM for an image resolution of $2^{11} \times 2^{11}$ if the accepted error is $\epsilon_0 = 0.1$ (corresponding to 186 iterations). We have arbitrarily chosen this value of ϵ_0 to obtain high-contrasted phase.
Note that the solution is not unique because there are often multiple possible solutions that can correspond to the same Fourier spectrum [13]. The image resolution δX is chosen to get a pixel size of the order of the pixel size of the phase-contrast microscope

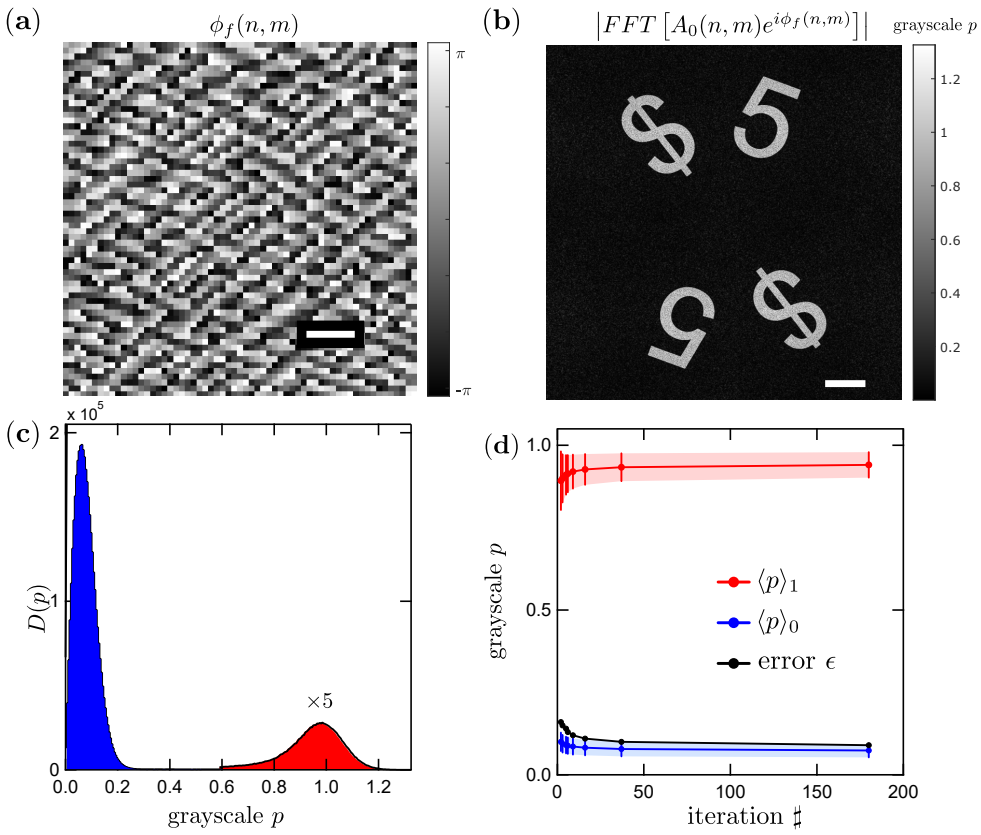

Figure 3. **(a)** Phase grating $\phi_f(n,m)$ corresponding to the target image, obtained using the Gerchberg–Saxton algorithm after 186 iterations. Scale bar: 100 µm. **(b)** Magnitude of $FFT\left[A_0(n,m)e^{i\phi_f(n,m)}\right]$ where $|A_0|^2 = I_0$ is the intensity of the collimated Gaussian beam with a 1.6 mm beam radius. Scale bar: 1 mm. **(c)** Histogram of the image in (b). The blue area corresponds to black pixels while the red one corresponds to the white pixels multiplied by a factor $\times 5$. **(d)** Black dots are error ϵ (see text) as a function of the number of iterations. Red (respectively blue) dots stand for the mean value of the red (respectively blue) distribution of the panel (c). The error bars stand for standard deviation.

image (1.82 µm/pixel, see Section 4). Figure 3(c) shows the distribution of grayscale values of Figure 3(b), namely the histogram. It essentially shows a peak centered on gray level 0 (blue) and another peak centered on gray level 1 (red). The greater the width of the blue (respectively red) peak, the darker (respectively light) gray levels there will be in the image: the histogram of a binary image is made up of only two infinitely fine peaks centered around zero and one. The greater the number of iterations of the algorithm, the smaller the width of the peaks approaching a binary image. Besides, the decrease in the standard deviation with the number of iteration of the red histogram indicates that we approach a black-and-white image (Figure 3(d)).

4. Grating structure of the Canadian banknote

In this section, we aim at comparing our numerical result to the real hologram, first qualitatively, and then quantitatively.

4.1. Phase-contrast microscopy of the banknote hologram

We first use a phase-contrast microscope to qualitatively observe the hologram of the banknote. In a phase-contrast microscope, the phase differences of light waves passing through different parts of the specimen are converted into visible intensity differences [22]. We use a Leica DM IRB with a 5x/0.12NA/Ph0 objective. A picture was taken with a Retiga6000 camera (Qimaging) using a binning of 2 which corresponds to a 1.82 µm pixel size. Figure 4(b) is part of this picture, displaying a part of the banknote diffractive hologram. This hologram is composed of alternating strips of different orientations, with each strip causing a different phase delay. This observed grating structure looks like the one reconstructed by the GS algorithm (Figure 3(a)).

4.2. Calculation of diffraction pattern of imaged phase-structure

The phase-contrast image (Figure 4(b)) and the calculated phase grating (Figure 3(a)) are not identical. To estimate their similarity, we measure the characteristic width of their strips by calculating the 2d spatial autocorrelation of both images. We start with the phase-contrast image $\varphi(n,m)$. To calculate its discrete autocorrelation function, we first consider the fluctuations:

$$\delta\varphi(n,m) = \varphi(n,m) - \langle\varphi\rangle, \tag{3}$$

where $\langle\varphi\rangle = \frac{1}{N\times N}\sum_{n=1}^{N}\sum_{m=1}^{N}\varphi(n,m)$ is the mean value of the phase-contrast image with $N = 2048$ pixels. We then calculate the Fourier transform of $\delta\varphi(n,m)$ by using the FFT algorithm (see Section 3). We finally compute the spatial autocorrelation $C(n,m)$ using the Wiener - Khintchine theorem [21]:

$$C(n,m) = \text{real}\left\{\text{FFT}^{-1}\left[\text{FFT}\left[\delta\varphi\right]\times\text{FFT}\left[\delta\varphi^{*}\right]\right]\right\} \tag{4}$$

where * denotes the complex conjugate. Figure 4(c) shows the 2d spatial autocorrelation of Figure 4(b): it exhibits a central peak whose width gives the characteristic size of the strips. To deduce the size ΔR of this peak, we calculate the radial autocorrelation function $C(r) = \frac{1}{2\pi r}\int_0^{2\pi} C(r\cos\theta, r\sin\theta)\,d\theta$ by summing the $C(n,m)$ values over a ring of radius r and thickness of one pixel. We find $\Delta R \simeq 18\,\mu$m, which is consistent with the characteristic size observed in Figure 4(b). We do the same analysis with the hologram obtained with the GS algorithm, $\phi_{\text{f}}(n,m)$, and find $\Delta R \simeq 26\,\mu$m (Figure 4(d)). The small discrepancy observed between the autocorrelation calculated on the hologram measured with the phase-contrast microscope and the hologram calculated with the GS algorithm is attributed to the difference in sampling size and the difference in the target image.

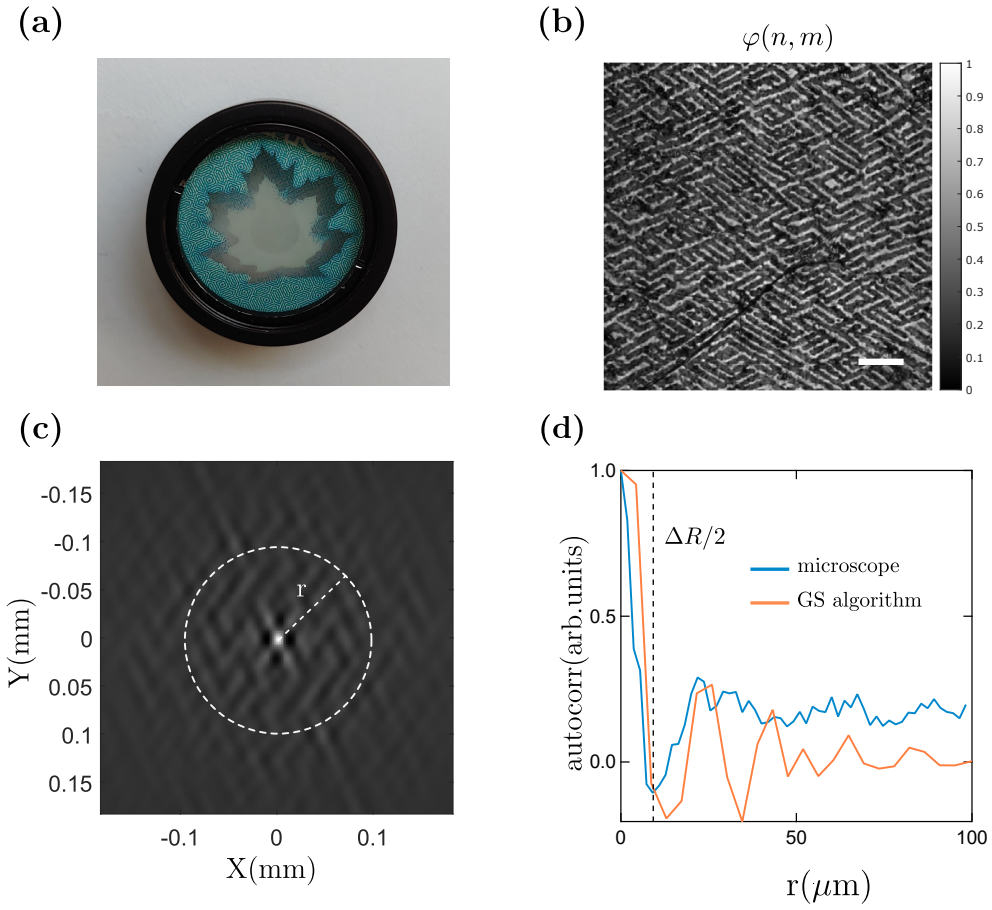

Figure 4. **(a)** One-inch optic mount holding the banknote piece containing the diffractive hologram hidden in the maple leaf of the $5 banknote (see Figure 1(a)). **(b)** Phase-contrast image $\varphi(n,m)$. Scale bar: 100 µm. **(c)** 2d spatial autocorrelation $C(n,m)$ of the image in (b). **(d)** 1d spatial autocorrelation function $C(r)$ corresponding to the radial average of $C(n,m)$ (blue curve, see text), exhibiting a typical length $\Delta R \simeq 20$ µm. The same analysis was done on the phase obtained with the GS algorithm (orange curve).

4.3. FFT of the observed grating structured

Last, we calculate the diffraction pattern of the observed phase-contrast image shown in Figure 4(b). We first superimpose this grayscale image and the Gaussian profile of the laser beam (red spot), as shown in Figure 5(a). By calculating the Fourier transform of this superposition, we obtain the diffraction pattern shown in Figure 5(b). We logically note a very good agreement between this pattern and the one we observed (Figure 1(d)).

5. Conclusion

We use two different experimental approaches to investigate the phenomenon of diffraction by a complex diffraction grating hidden in a banknote. In both cases, we use numerical tools based on the Fourier transform to explore the link between a small-scale

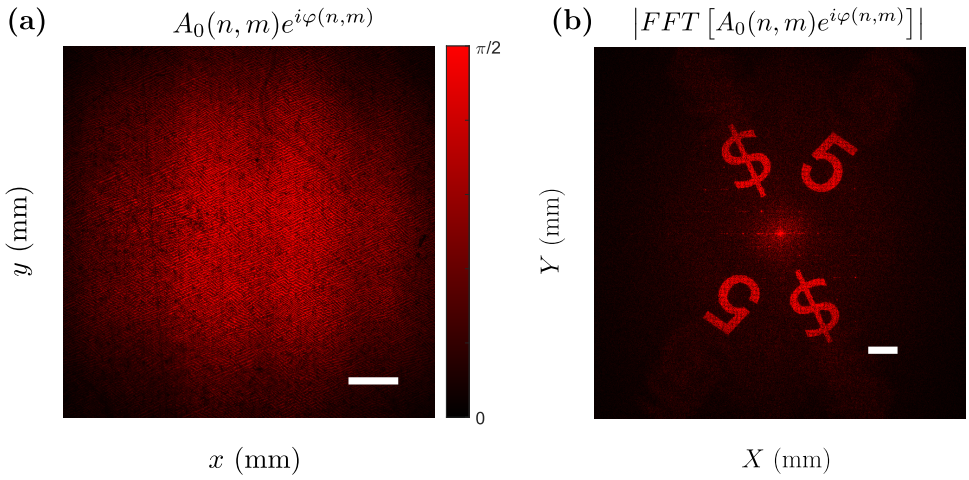

Figure 5. (a) Superposition of the phase-contrast image $\varphi(n,m)$ and the $w = 1.6\,\text{mm}$ laser spot $A_0(n,m)$. Scale bar: $500\,\mu\text{m}$ **(b)**. Magnitude of the FFT of $A_0(n,m)e^{i\varphi(n,m)}$. Scale bar: $1\,\text{mm}$

structure and its diffraction pattern. These experimental and numerical investigations have shown how to deduce a grating structure based on its given diffraction pattern. By providing some insight into the relationships between diffractive structures and diffraction patterns, we believe this work will benefit students in their understanding of diffraction and Fourier transforms.

We are convinced this study can be performed by undergraduate students at university level to get a wider understanding of diffraction theory by highlighting the importance of the phase of the optical signal. Besides, such experiments enable students to work with image processing and numerical computation.

Acknowledgement We are grateful to F. Bouquet and A. Buguin for their reading of the manuscript and suggestions.

References

[1] John Crace (2013), *Banknotes: a short history*. Available at `https://www.theguardian.com/business/2013/sep/10/banknotes-history` (Accessed: 07 February 2023).

[2] Fisher-Høyrem, Stefan, " Banknotes: The Money of Civilization - Rethinking Secular Time in Victorian England", (Springer International Publishing), page 165–218 (2022).

[3] Klaus W. Bender, *Moneymakers: The Secret World of Banknote Printing*, (John Wiley & Sons, 2006).

[4] M. Mann, S Shukla and S. Gupta, "A comparative study on security features of banknotes of various countries", *Int. J. Multidiscip. Res. Dev*, 2:83–91, (2015).

[5] A. Centeno, O. Terrades, J. Canet and C. Morales "Identity Document and banknote security forensics: a survey", *arXiv:1910.08993* (2019).

[6] B. A. Hardwick, Performance of the diffraction grating on a bank note: the experience with the Australian Commemorative note," SPIE 1210, Optical Security and Anticounterfeiting Systems, (1990).

[7] E. Prime and D. Solomon, Australia's Plastic Banknotes: Fighting Counterfeit Currency," *Angewandte Chemie International Edition*, 49: 3726-3736 (2010).

[8] Richard P. Feynman, Robert B. Leighton, and Matthew Sands, *The Feynman Lectures on Physics, Vol. 1* (The New Millenium edition, 2010), chapter 30.

[9] W.L. Bragg (1922), *Nobel Lecture*. Available at `https://www.nobelprize.org/uploads/2018/06/wl-bragg-lecture.pdf` (Accessed: 07 February 2023).

[10] Pablo Aguilar-Marín, Luis Angelats-Silva, Ernesto Noriega-Diaz, Mario Chavez-Bacilio and Ricardo Verde-Vera, *Eur. J. Phys.* **41** 045501 (2020).

[11] R.F. Franklin and R.G. Gosling, "Molecular Configuration in Sodium Thymonucleate," *Nature* **171** pages 740–741 (1953).

[12] E. Hecht, *Optics* (Pearson Education, 2017), chapter 10.

[13] R.W. Gerchberg and W. O. Saxton, "A Practical Algorithm for the Determination of Phase from Image and Diffraction Plane Pictures," in *Optik* **35**, 237 (1972).

[14] J.W. Cooley et J.W. Tukey, " An algorithm for the machine calculation of complex Fourier series," in *Math. Comp.* **19**, 297-301 (1965).

[15] S. Mould (2015), *Plastic Banknotes and lasers.* Available at `https://www.youtube.com/watch?v=iMGvTYDC5MA(Accessed:07February2023).`

[16] J. Bobroff (2024), *Le trésor caché du 5 $ canadien.* Available at `https://www.youtube.com/watch?v=yKbuajreIGw(Accessed:07February2023).`

[17] Bank Of Canada (2013), *$5 polymer note*. Available at `https://www.bankofcanada.ca/banknotes/bank-note-series/frontiers/5-polymer-note/` (Accessed: 07 February 2023).

[18] Jackson J. D., Classical Electrodynamics (New York: Wiley, 3rd Edition 1975), chapter 10.

[19] M A C Potenza. "An extremely simplified optics laboratory for teaching the fundamentals of Fourier analysis," in *Eur. J. Phys.* **42**, 035304 (2021).

[20] J.W. Goodman, *Introduction To Fourier Optics* (Roberts and Company Publishers, 2004).

[21] J. M. Giron-Sierra, *Digital Signal Processing with Matlab Examples, Volume 1*, Appendix 2.4.

[22] I. Bányász, " Direct measurement of the refractive index profile of phase gratings, recorded in silver halide holographic materials by phase-contrast microscopy," in *App Phys Letters* **83**, 4282 (2003).